# Some aspects of the deep abyssal overflow between the middle and southern basins of the Caspian Sea

**Javad Babagoli Matikolaei[1], Abbasali Aliakbari Bidokhti[2], and Maryam Shiea[3]**

[1]Graduate in Physical Oceanography, Institute of Geophysics, University of Tehran, Tehran, Iran.
[2]Institute of Geophysics, University of Tehran, Tehran, Iran.
[3]Faculty of Marine Science and Technology, Science and Research Branch, Islamic Azad University, Tehran, Iran.

*Correspondence to*: Abbasali Aliakbari Bidokhti(bidokhti@ut.ac.ir)

**Abstract.** This study investigates the deep gravity current between the middle and southern Caspian Sea basins, caused by density difference of deep waters. Oceanographic data, numerical model and dynamic models are used to consider the structure of this Caspian Sea abyssal overflow. The CTD data are obtained from UNESCO, and the three-dimensional ocean model COHERENS results are used to study the abyssal currents in the southern basin of the Caspian Sea.

The deep overflow is driven by the density difference mainly due to the temperature difference between the middle and southern basins especially in winter. For this reason, water sinks in high latitudes and after filling the middle basin it overflows into the southern basin. As the current passes through the Absheron Strait (or sill), we use an analytic model for the overflow gravity current with inertial effects, bottom friction and entrainment, to consider its structure. The dynamical characteristics of this deep baroclinic flow are investigated with different initial and boundary conditions. The results show that after time passes, the flow adjusts itself, moving as a deepening gravity driven topographically trapped current. This flow is considered for different seasons and its velocity and width are obtained. Because of the topography of the Southern Caspian basin, the flow is trapped after the sill; thus, another simple dynamical model of the overflow, based on potential vorticity similar to that of Bidokhti and Ezam (2009) but with the bottom friction and entrainment included, is used to find the horizontal extent of the outflow from the western coast. To estimate the changes of vorticity and potential vorticity of the flow over the Absheron sill, we use the method of Falcini and Salusti (2015), in this work, the effects of entrainment and friction are considered. Because of the importance of the overflow in deep water ventilation, a simple dynamical model of the boundary currents based on the shape of strait is used to estimate typical mass transport and flushing time which is found to be about 15 to 20 years for the southern basin of the Caspian Sea. This time scale is important for the possible effects on the ecosystem here of pollution due to oil exploration.

**Keywords:** Overflow, dynamical model, trapped baroclinic bottom current, Caspian Sea abyssal flow.

## 1.Introduction

Baroclinic flows play important roles in ocean and sea circulations, especially in deep waters of the ocean. Because these currents are important in deep water ventilations of the oceans, they have an integral role in thermocline circulation. Vertical ocean circulation that is created by density differences and controlled by changes in surface temperature and salinity is known as thermohaline circulation. A driving mechanism for the circulation is the cooling of surface waters at high latitudes and consequent formations of deep waters by sinking the cooled salty water masses (Fogelqvist et al.,2003).

Cooling in polar seas (Dickson et al., 1990) and evaporation in marginal seas (Baringer and Price, 1997) cause dense waters that sink to form deep water masses. For example, dense water from the deep convective regions of the North Atlantic produces a signature of the thermohaline overturning circulation that can be seen as far away as the Pacific and Indian oceans (Girton et al., 2003). In the global sense, bottom-trapped currents play an integral role in thermohaline circulation and are a vehicle for the transport of heat, salt, oxygen and nutrients over great distances and depths. The ability of abyssal flows to transport and deposit sediments is also of geological interest (Smith, 1975). As thermohaline circulation causes ventilation of deep ocean water, it is important not only in open seas and ocean but also in semi-closed and closed basins ventilations, e.g. the Caspian Sea. Study of thermohaline dynamics and circulation has also been of interest to other scientists such as climate researchers. The dynamics of such dense currents on slopes have been modelled in the past both theoretically and experimentally starting with Ellison and Turner (1959) and Britter and Linden (1980), and a review on gravity currents can be found in Griffiths (1986).

Bidokhti and Ezam (2009) presented a simple dynamical model of the outflow from the Persian Gulf based on potential vorticity conservation to find the horizontal extent of the outflow from the coast.

The Caspian Sea, the world's largest inland enclosed water body, consists of three basins namely northern(shallow, mean depth of about 10 m and covering 80000 km$^2$), the middle (rather deep, with mean depth of about 200 m, maximum depth 788 m and covering 138000 km$^2$) and the southern (deep, with a mean depth of 350 m, maximum depth 1025 m and covering 164840 km$^2$) and is located between 36.5 Nand 47.2N, and 46.5E and 54.1E (Aubrey et al., 1994; Aubrey, 1994). The depth varies greatly over this sea (Ismailova, 2004, Figure 2). The northern basin, after a sudden depth transition at the shelf edge, reaches the middle one. The middle and southern basins are divided by the Absheron sill or strait (with maximum depth of 180m).The western slopes of the two deeper basins are fairly steep compared to the eastern slope (Gunduz and Özsoy, 2014). Peeters et al (2000) have also estimated the ages of waters of the Caspian Sea basins while considering the exchange between the middle and southern basins, based on chemical tracers and found typical ages of about 20 to 25 years depending on the exchange rates. This exchange rate seems to vary year by year that is dominated by atmospheric forcing.

The Caspian Sea is enclosed with tides being fairly weak and circulation in this sea is mainly due to wind and buoyancy, although some wave-driven flows also occur in coastal regions [Bondarenko, 1993; Ghaffari and Chegini, 2010; Ghaffari et al., 2013; Ibrayev et al., 2010; Terziev et al., 1992].The seasonal circulation based on a coupled sea hydrodynamics, air–sea interaction and sea ice thermodynamics model of the Caspian Sea was investigated by Ibrayev et al(2010) and Gunduz and

Özsoy, 2014).The effect of fresh water inflow to the Caspian Sea on seasonal variations of salinity and circulation (or flow) pattern of the Caspian Sea surface has also been studied using HYCOM model (Kara et al, 2010). These studies indicate that in north-eastern parts of the middle basin of this sea there are signs of sinking water in cold season. Such deep convection can lead to thermocline convection affected by side topography of these basins (middle and southern basins). These deep topographically influenced rotating flows constitute the abyssal circulation of the Caspian Sea.

The main aim of our work is to investigate some aspects of the abyssal flows in the southern Caspian Sea basin using CTD data and some simulations of a numerical model. Firstly, we explain why abyssal circulation can occur in the Caspian Sea, and then discuss the structure of the outflow (overflow) from the middle to the southern Caspian Sea over the Absheron sill. An analytical model for the overflow gravity current over the Absheron sill, with inertial and frictional effects is then presented. After the flow passes over the Absheron sill, we present a new model for the structure of this flow using another analytical model based on potential vorticity, similar to that of Bidokhti and Ezam (2009) but the bottom friction and entrainment is included. We then calculate values of mass transport flushing times, and discuss the pathway of gravity current in southern Caspian Sea basin.

## 2 Data used and results

### 2.1 Observational data

The sea surface temperature (SST) in the northern basin ranges from below zero under frozen ice in winter to 25–26 °C in summer, while more moderate variability occurs in the southern basin changing from 7–10 °C in winter to 25–29 °C in summer (Ibrayev et al., 2010). To illustrate the differences of surface temperatures of the middle, southern, and northern basins in various seasons, time series of surface temperatures are plotted using MODIS data from 2014 to 2015 in figure 1.These data are hourly data, so the temperature values are slightly different from the average value mentioned by Ibrayev et al., 2010. In winter, the surface temperature difference between the northern and southern basin is approximately 16 °C. Apart from this, the Caspian Sea has low salinity. In deep water areas, salinity varies little with depth (12.80–13.08 psu), and the density stratification largely depends on temperature variation (Terziev et al., 1992). Hence, denser water of the middle basin, in comparison to that of the southern basin, is expected as will now be shown.

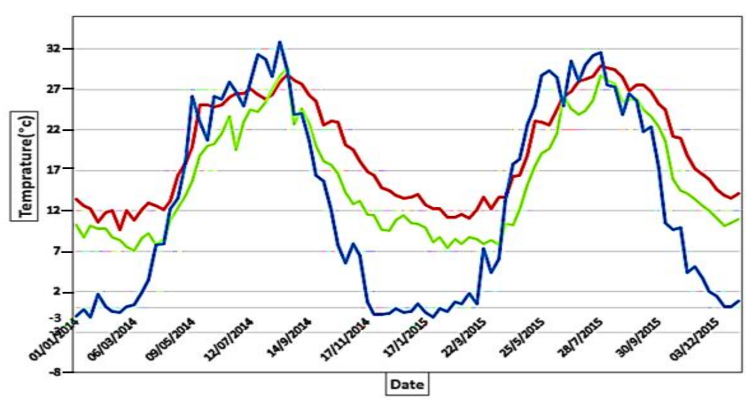


**Figure 1:** Comparison the surface temperature in Northern (Lat: 46.5°, Long: 50°) (blue), Middle (Lat: 39.5°, Long: 51°) (green), and Southern (Lat: 37°, Long: 52°) (red), basins of the Caspian Sea.

The CTD data are obtained from UNESCO Atomic Energy International Agency, forsummer1996 (Figure 2). Vertical profiles of temperature, *T*, salinity, *S* and sigma-*T*, for the northern, middle, and southern Caspian Sea basins, show differences in temperature, salinity and sigma-*T* between these basins. Figure 3 shows typical vertical profiles of *T*, *S* and sigma-*T* in these basins (points a and b in Figure 2 right). Due to the density difference between the middle and southern basins, dense current crosses the Absheron sill. The cross-section of sigma-*T* shows that the abyssal gravity current moves from middle to southern basin (Figure 4). In order to further illustrate the location of Figure 4,  it should be mentioned  that the depth of water in this area is about 180 to 200 meters and the nearest distance of measured data is about 80 km from the coast of Azerbaijan

Due to the limited observational data, more extensive measurements and high resolution data are required to find the outflow structure and determine the analytical model parameters. For this reason, numerical model results have been used to do further analyses and also acquire the parameters of the overflow for the analytical model.

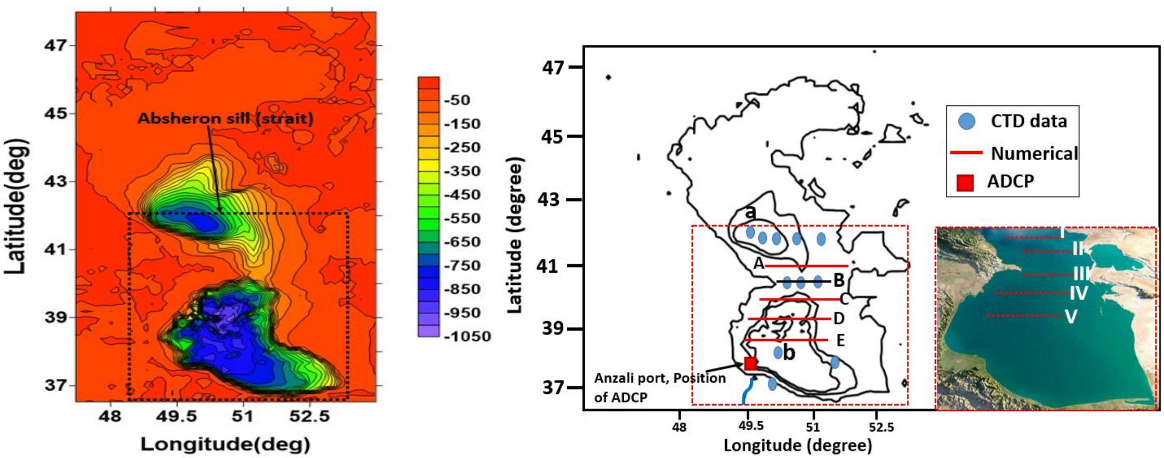


**Figure 2:** Schematic of the Caspian Sea and locations of CTD and ADCP measurements, the geographic position of transects (right), and topography of the basins, showing the Absheron sill (left).The cross- sections marked with Greek letters are pointed out in section3.2.1. The purpose of bringing the figure here is to compare the location of two cross-sections D and V.

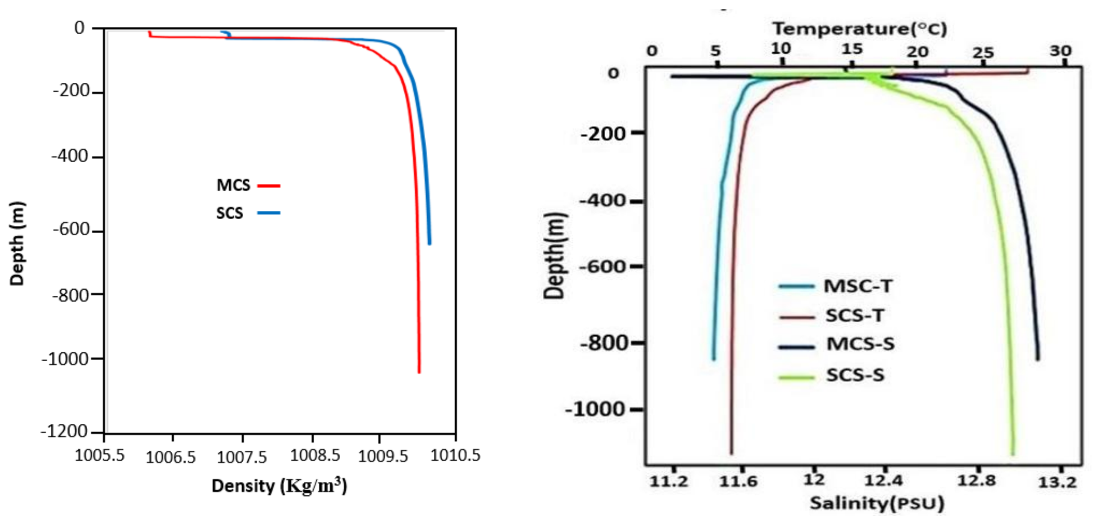


**Figure 3:** Comparison Salinity, *S* and temperature, *T* (right), and density (left) profiles between points a, in middle (MCS) and b, in southern (SCS) Caspian Sea basins (Figure 2 right).

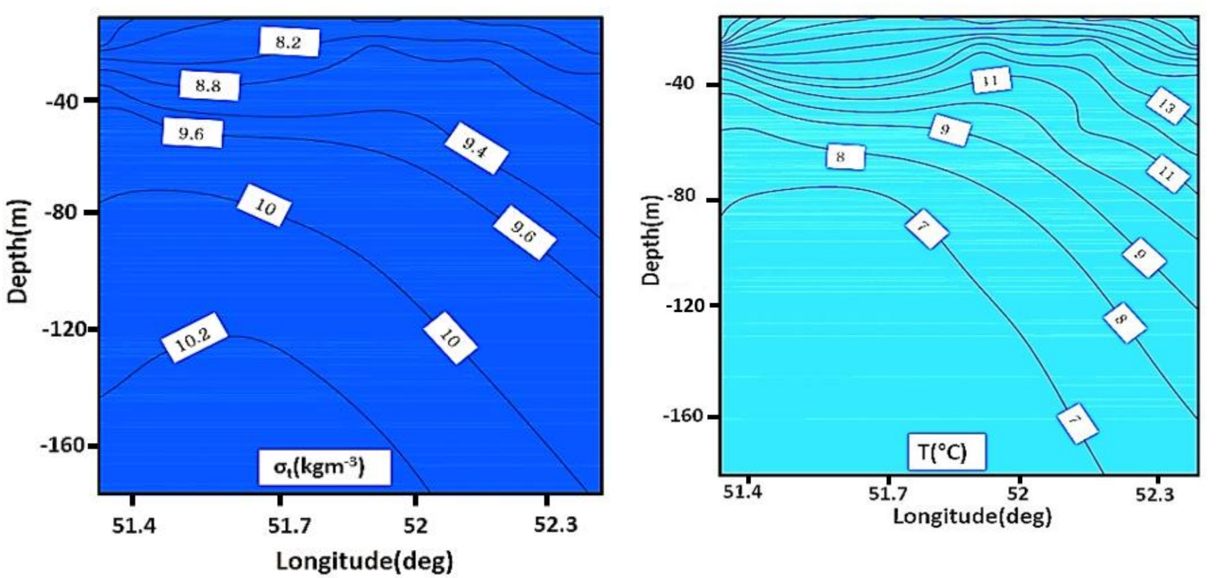


**Figure 4**: Observed sigma-*T* (left) and temperature (right) fields along transect B in summer, shown in Figure 2 right.

### 2.2 Some general features of the COHERENS numerical model, and its boundary and initial conditions

Here the COHERENS (Coupled Hydrodynamical Ecological model for Regional Shelf seas; Luyten et al., 1999) has been used. COHERENS uses a vertical sigma coordinate and the hydrostatic incompressible version of the Navier-Stokes equations with Boussinesq approximation and equations of temperature and salinity. The model uses an Arakawa C-grid (Arakawa and Suarez, 1983) and equations are solved numerically using the mode-splitting technique. The grid size in horizontal is 0.046 × 0.046 degrees, typically 5 km, and 30 sigma layers, labelled k (the bottom layer is 1 and surface one is 30). The coastlines and bathymetry data with 0.5º ×0.5º resolution are acquired from GEBCO, although interpolated and smoothed slightly.

The model was initialized for winter (January) using monthly mean temperature and salinity climatology obtained from Kara et al (2010); and it was forced by six hourly wind, acquired from ECMWF (Mazaheri et al., 2013), and air pressure and temperature with 0.5˚×0.5˚resolution acquired from ECMWF (ERA-Interim) reanalyses. Precipitation rate, cloud cover and relative humidity (2.5˚×2.5˚) were derived from NCEP/NCAR re-analysis data. The river inflows (from the Global Runoff Data Centre) were also included. The time steps of barotropic and baroclinic modes are 15 s and 150 s respectively. The total simulation time is five years (from 2000 to 2004 inclusive) with six hour varying meteorological forcing and then the results of the last year are shown. The results of numerical model are validate by ADCP data between the estuary of the Sefidrood River and Anzali port (figure 2, 5). These data are collected by National Institute of Oceanography and Atmospheric Sciences, from November 2004 to the end of January 2005 (Shiea et al., 2016).This data was recorded by RCM9 current meters (at the ADCP station) at 3 depths on a mooring, near surface, 50 m, and 200 m.The simulation results of mean and long period variations of surface velocity components are rather consistent with observations. The difference in velocity between observation and model comes from some of the assumptions and the resolution used in the model as can be expected. The distance between two adjacent grid points in model is about 5 km and the ADCP data are a point in between two grid points, so interpolation are used to compare the model results with data of the point of observations.

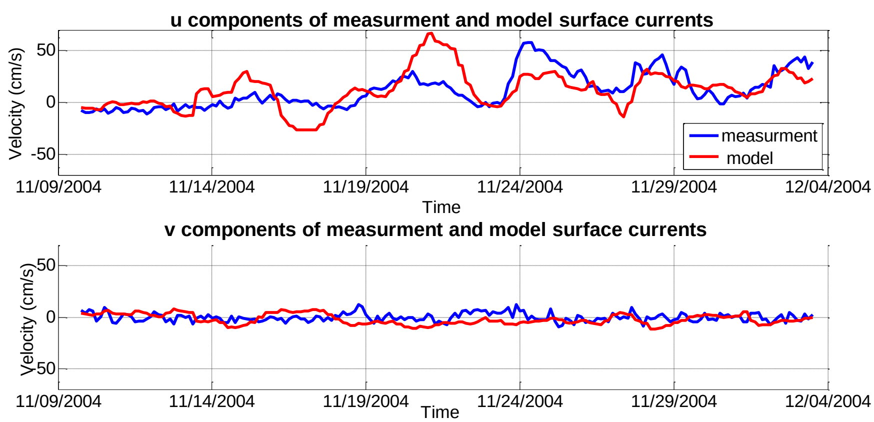


**Figure 5**: Comparison between numerical model results of surface current components and observation near the Sefidrood River and Anzali port (Shiea et al., 2016).

Typical numerical results of deep flows for the middle and southern basins of the Caspian Sea (the flow for the northern basin is not shown) for May and December of 2004, after four years of warm up of the model operation, are shown in Figure 6,7 and 8. The deep narrow flow in the middlebasin and the overflow over the Absheron sill and in the north western boundary of the southern basin are clearly observed. As the northern shallow waters of the Caspian Sea are subjected to high evaporation in summer, in the following cold seasons these waters become dense and start to sink, mainly in the north eastern side (Gunduz and Özsoy, 2014), into the middle basin(figure 6) . The flow due to its high density enters the deep part of the middle Caspian and starts to fill the middle Caspian Sea basin. After filling the middle Caspian basin, it appears to overflow into the southern basin, due to shape of Absheron strait that looks like a sill similar to Denmark Strait. This enters the southern Caspian Sea through Absheron strait. The topography has a strong effect on the deep basin flows. From such results the parameters of the deep flow are derived. There is a clear indication that the heavier water of the middle basin is overflowing near the bottom left towards the southern basin (figure 8, 9). For comparison between the results of the numerical model and observation data based on Fig.7, it indicates that the numerical model shows higher temperature than that of observation data at the same depth. For example, if we consider potential temperature of 6 degrees Celsius (see Fig. 7, isothermal line), its isothermal line is at a depth of 200-300 in the numerical model, and this value isotherm is at about 200-250 m based on observation data. The reasons for this can be due to the fact that the results from the numerical model (2004) and observation data (1996) are generally for different years. Apart from this, Observation data is for about one day and at a certain time, but the numerical model is averaged over a month (corresponding month i.e. September) and also the number of measured points is much less than those of the numerical model results. On the other hand, the Absheron strait is shallow, hence weather forcing are significant and effective on the structure of temperature. As a result, in this area, we did not try to compare the numerical model simulations with observation data in terms of the identical position of the isothermal line. We intend to justify that the numerical model simulations are rather accurately predicted and field data confirms this rather well. Due to lack of field data, we used the numerical model simulations as well as the limited observation data in this paper.

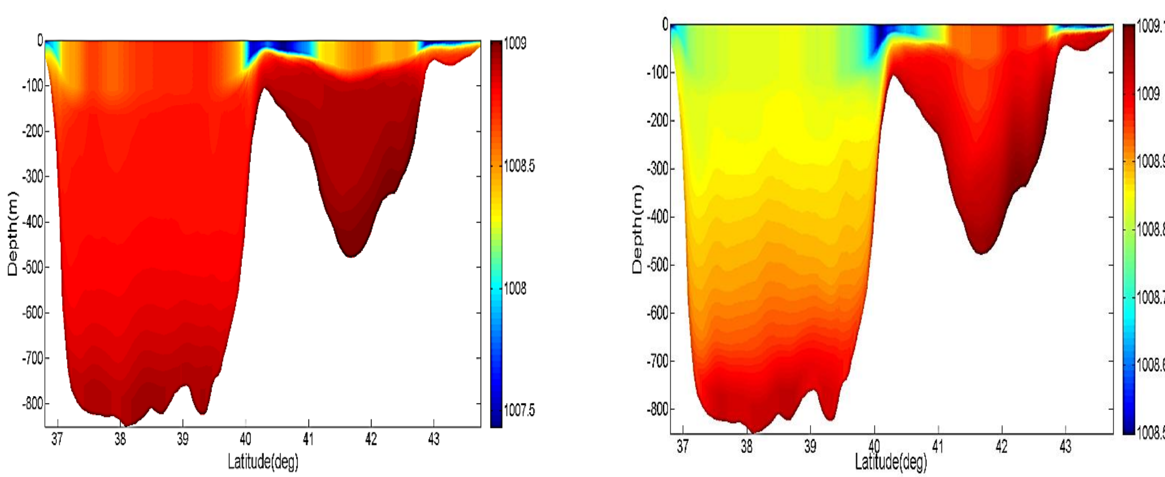


**Figure 6:** Cross-Section (N-S) of the mean density obtained from model simulation during September (left) and May (right).

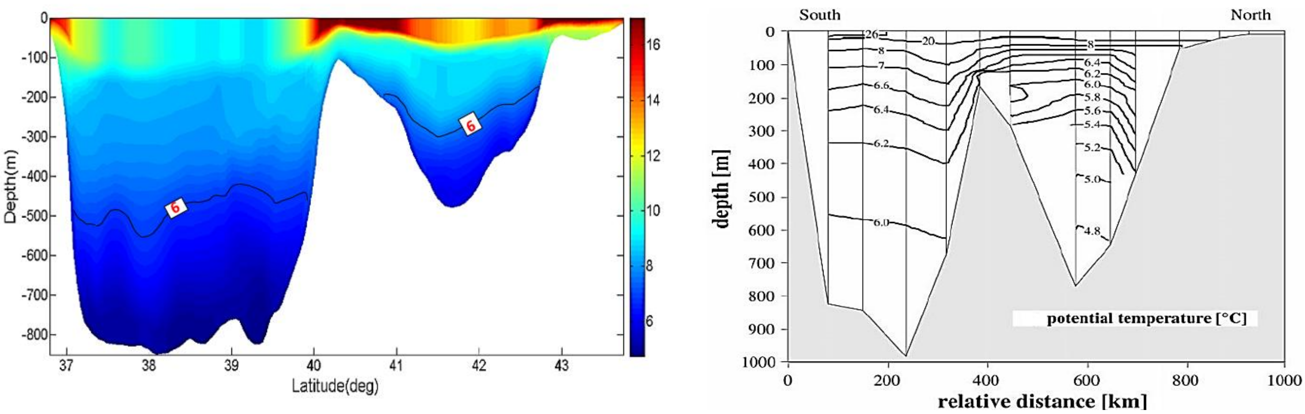


**Figure 7:** Comparison between cross-sections (N-S) of the mean temperature obtained from model simulation (left) and Peeters et. al (2000) measurements (right) during September. The isotherms of 6 °C are remarkably similar in numerical model simulation and observational data.

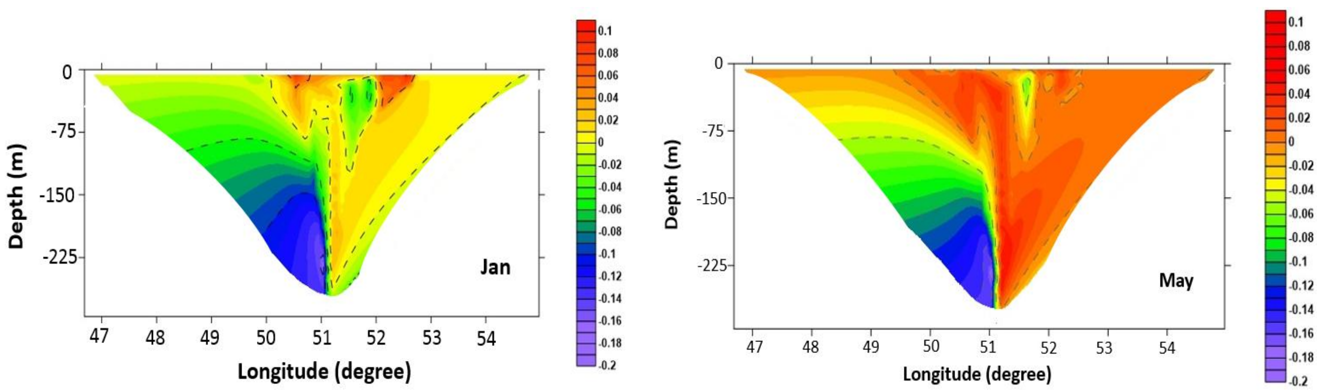


**Figure 8:** Cross-Section of the mean velocity (m/s) in transect A (left, for Jan.) and C (right, for May) obtained from model simulations.

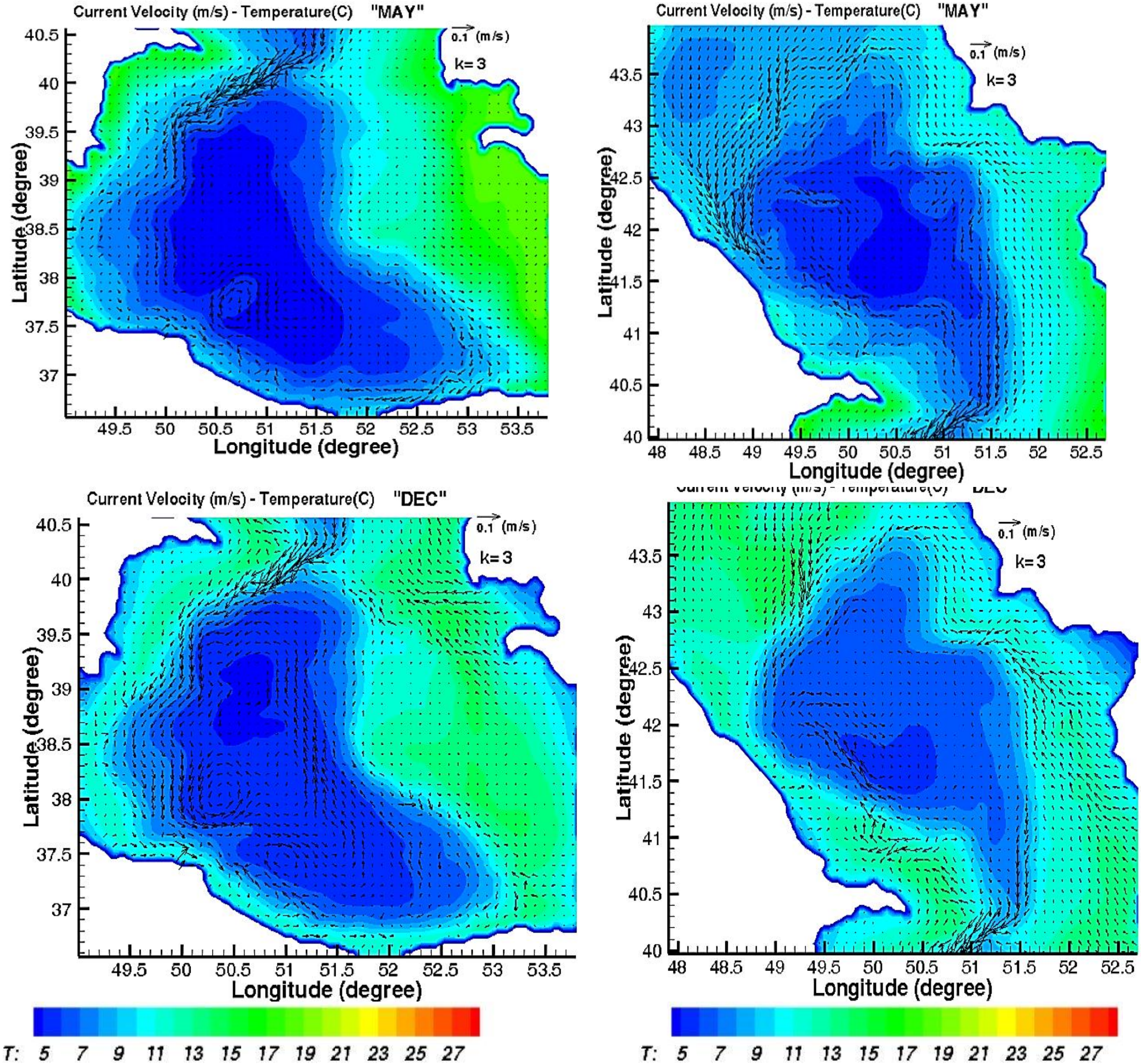


**Figure 9:** Monthly mean currents (m/s) in layer "k=3" (near the bottom) and temperature obtained from model simulations in southern (left) and middle (right) basins of the Caspian Sea for the months of May, December (2004).

The deep flow seems to follow the bottom topography, indicating that the bottom slopes of the middle and southern basins strongly influence the abyssal circulation. This in fact led us to propose an analytical model for the density current on a sloping bottom affected by bottom friction and entrainment, hence, spiralling into the deep parts of the southern Caspian Sea basin. Typical Rossby number of this flow is about $Ro = \frac{U}{fW} = 0.2/(10^{-4} \times 20 \times 10^{3}) \sim 0.1$ (here $U$ is typical speed of the overflow and $W$ is its width), which justifies the geostrophic flow (assumption) entering the southern basin.

## 3 Dynamics of the overflow

### 3.1 An analytical model for the overflow in the Strait

As the gravity current flows over the inclined sill, it adjusts itself under the gravitational, rotational and frictional forces. The zonal and meridional components of momentum of the buoyancy driven current are given by assuming no pressure gradient; a uniform dense flow under a less dense layer at rest; $x$ coordinate is eastward (directed along the slope) and y is northward (y perpendicular to slope, see Figure 10); with entrainments at its boundaries, E(here solely as a frictional factor otherwise the flow becomes three dimensional and a similarity method would be suitable) and with bottom friction, $\tau_b$; under these simplifying assumptions, the continuity equation is trivial and hence, the required momentum equations for the solution are:

$$\frac{du}{dt} = fv - \frac{\tau_{bx}}{\rho H} - \frac{E}{H}u$$
$$\frac{dv}{dt} = -fu - g'\tan\theta - \frac{\tau_{by}}{\rho H} - \frac{E}{H}v \qquad \textbf{(1)}$$

Where $u$ and $v$ are Lagrangian eastward and northward components of velocity respectively (Figure 10), $f$ is the Coriolis parameter (= 2Ω sin $\upsilon$, where $\Omega$ is the earth angular speed, and υ is the latitude angle),calculated as $f \sim 9.2\times10^{-5}\mathrm{s}^{-1}$.$\theta$ is the bottom slope angle and here tan $\theta$=0.02, $g'$ is the reduced gravity, values of reduced gravity were calculated for different seasons (see table 2) and $H$ is the depth of overflow (thickness of the overflowing layer), about 50 to 70 m. The stress on the ocean bottom, $\tau_b$, is parameterized by the usual quadratic form, $\tau_b = \rho C_d|U|u$ *or* $v$ where $C_d$ is drag coefficient and $U$ is the magnitude of velocity. To simplify the analysis, we define$r_b = \frac{C_d|U|}{H}$ and$r_e = \frac{E}{H}$.The solutions of these differential equations are as follows: (where $x$ and $y$ are Lagrangian location coordinates of the flow and $c_1$and $c_2$are constants to be found from initial conditions, see Table 2below).

$$u(t) = c_1 e^{-(r_b+r_e)t}\cos(ft) + c_2 e^{-(r_b+r_e)t}\sin(ft) - \frac{g' f \tan\theta}{f^2 + (r_b + r_e)^2}$$
$$v(t) = -c_1 e^{-(r_b+r_e)t}\sin(ft) + c_2 e^{-(r_b+r_e)t}\cos(ft) - \frac{g'(r_b + r_e)\tan\theta}{f^2 + (r_b + r_e)^2} \qquad \textbf{(2)}$$

$$x(t)=\frac{fc_1-(r_b+r_e)c_2}{f^2+(r_b+r_e)^2}e^{-(r_b+r_e)t}\sin(ft)-\frac{fc_2+(r_b+r_e)c_1}{f^2+(r_b+r_e)^2}e^{-(r_b+r_e)t}\cos(ft)-\frac{g'f\tan\theta}{f^2+(r_b+r_e)^2}t+\frac{fc_2+(r_b+r_e)c_1}{f^2+(r_b+r_e)^2}$$

$$y(t)=\frac{fc_2+(r_b+r_e)c_1}{f^2+(r_b+r_e)^2}e^{-(r_b+r_e)t}\sin(ft)+\frac{fc_1-(r_b+r_e)c_2}{f^2+(r_b+r_e)^2}e^{-(r_b+r_e)t}\cos(ft)-\frac{g'(r_b+r_e)\tan\theta}{f^2+(r_b+r_e)^2}t+\frac{(r_b+r_e)c_2-fc_1}{f^2+(r_b+r_e)^2}$$

Where:

$$c_2=v_p+\frac{g'(r_b+r_e)\tan\theta}{f^2+(r_b+r_e)^2}$$
$$c_1=u_p+\frac{g'f\tan\theta}{f^2+(r_b+r_e)^2} \qquad \textbf{(3)}$$

$u_p$ and $v_p$ are components of velocity when the gravity current just begins to flow over the inclined sill.

As the time passes, the flow tends to reach a steady state and moves parallel to the sloped bed. Then in this situation $v_{t\to\infty}$ and $u_{t\to\infty}$are obtained from the following equation in which $\mu$ is the flow angle from zonal east-west direction and $\lambda$ is its initial value.

$$u_{t\to\infty}=-\frac{g'f\tan\theta}{f^2+(r_b+r_e)^2},v_{t\to\infty}=-\frac{g'(r_b+r_e)\tan\theta}{f^2+(r_b+r_e)^2}$$
$$\tan\mu=\frac{v_{t\to\infty}}{u_{t\to\infty}},\mu=\arctan(-\frac{r_b+r_e}{f}) \qquad \textbf{(4)}$$
$$\tan\lambda=\frac{v_p}{u_p},\lambda=\arctan(\frac{v_p}{u_p})$$

As the flow develops with time it shows some oscillations with the local inertial period, and after a few inertial periods it acquires a steady state velocity namely $u_{t\to\infty}$ and $v_{t\to\infty}$. The analytical model input parameters (see Table 2 below) were determined from observations (cross-sections shown in Figure 4) and numerical simulations in the Strait of Absheron,from the cross-sections as shown in Figure11.

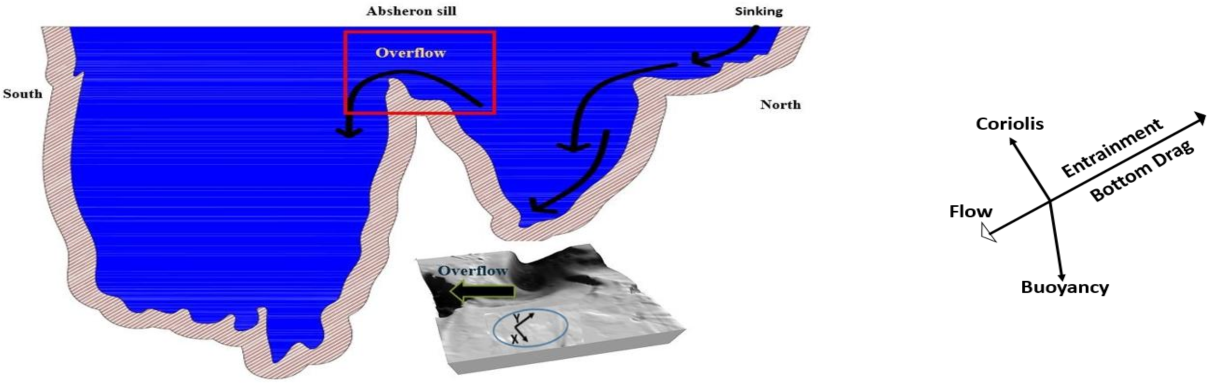


**Figure10:** A schematic diagram of the sinking flow in the middle basin and the overflow current over Absheron sill (top),and topography around the sill in the middle of the Caspian Sea with the chosen coordinates (bottom).

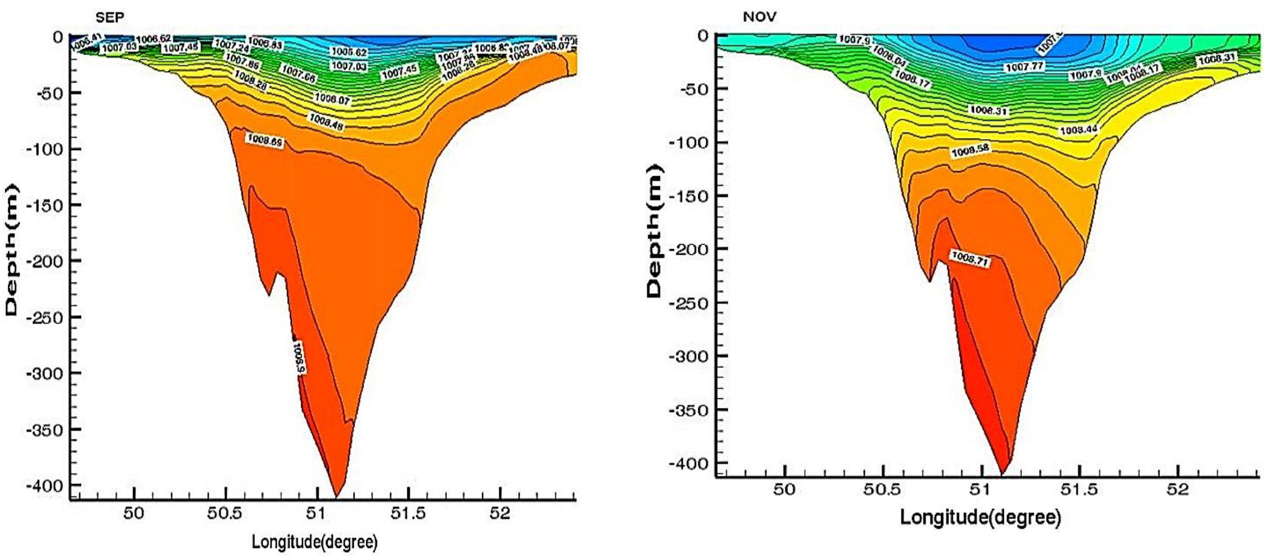


**Figure11**: Simulated density fields along transect C in Sept. and Nov. 2004.

### 3.1.1 Estimation of drag coefficient and entrainment parameter

Johnson and Sanford (1992) estimated $C_d$=3×10$^{-3}$ from the analysis of data from the Mediterranean outflow. Girton and Sanford (2003) used $C_d$=3×10$^{-3}$ for Denmark Strait and Cheng et al (1999) studied the bottom roughness length and bottom shear stress in South San Francisco Bay and calculated $C_d$ from 2×10$^{-3}$ to 6×10$^{-3}$. In this study we have conducted the analysis using $C_d$=3×10$^{-3}$ and 5×10$^{-3}$. Hence, $r_b = C_d\, u / H$=0.003×0.2/50 ~ 1 ×10$^{-5}$1/s and $r_b = C_d u/H$=0.005×0.2/50 ~ 2×10$^{-5}$ 1/s. $u_E$ is an entrainment speed and defined as $u_E = E^* \times U$ where $E^*$ is entrainment parameter that depends on a function of the layer Richardson number (Price and Bringer, 1994). $Ri$ is the bulk Richardson number defined as $Ri = \frac{g'H}{U^2} cos\theta$, with $U$ being the amplitude of layer velocity, $\theta$ is the bottom slope. There are many methods to calculate $E^*$ of which some are presented in table 1. Based on $Ri$ for the outflow and due to the fact that $Ri$ varies at different locations, we use two values for $r_e$. Using $U$ as 0.1 to 0.2 m/s, $g'$=0.00222-0.00251m/s$^2$, $H$=50-70 m, tan $\theta$=0.02, $Ri = \frac{0.00251 \times 50}{0.2 \times 0.2}$ 0.99~ 3.1. Based on table 1 and $Ri$ >0.08, we used mean $E^*$ based on formulas 2, 3, 4 and 5. For this section, $r_e$ values are considered as $5\times10^{-6}$ and $1\times10^{-5}$ based on typical value for $Ri$, $U$ and $H$.

**Table 1:**Some of the published $E^*$ equations based on $Ri$ (Kashefipour et al, 2010)

| Equation number | Researcher | Year | Equation |
|---|---|---|---|
| 1 | Ellison and Turner | 1959 | $E^*=\frac{0.08-0.1Ri}{1+5Ri}$ |
| 2 | Ashida and Egashira | 1977 | $E^*=0.0015Ri^{-1}$ |
| 3 | Garcia | 1985 | $E^*=\frac{0.075}{(1+718Ri^{2.4})^{0.5}}$ |
| 4 | Kessel and Krancnburg | 1996 | $E^*=\frac{5.5\times10^{-3}}{3.6Ri-1+\sqrt{(3.6Ri-1)^2+0.15}}$ |
| 5 | Karamzade | 2004 | $E^*=0.0021\,Ri^{-1.1238}$ |

### 3. 1.2 *The result of the analytical model*

Figures12 and 13show that as the flow passes through the Strait, due to the Coriolis force it is deflected to the right. If initial velocity is greater, it moves farther along the meridian. The results show that at later times (especially for larger $r_b$ and $r_e$) the flow moves a shorter distance in longitude and the direction of flow loses its sinusoidal oscillations (Figure12 and Table 2). According to Table 2, the angle between the velocity and eastward is increased when compared with the initial velocity. After an initial acceleration, the flow oscillates a few times before adjusting to a flow at a small angle to the isobaths, depending on the bottom friction coefficients and entrainment (Figures 12and13).The results are based on uniform sloped bottom in the southern basin and initially the flow moves over the ramp. However, due to the bottom topography in southern basin and the narrow Apsheron strait and it is estimated that the flow is trapped after about 10 km downstream.

Due to a bottom slope of $\theta$=0.02, the flow sinks approximately 180-200 m in the southern basin, as the numerical model confirms (Figures 6 and 7). For example, if we consider isothermal of 6.2 ° in observation data (Fig.7) the water sinks about 200 m after the strait. Based on numerical simulations, as in the Fig. 7, the water sinks about 200-250 m. To determine its sinking value exactly, it should be better to use another method because the flow does not exactly move the North-South direction (Fig.9). If it is calculated based on the changes in isopycnal in transect A and C (Fig. 11 and 19, isopycnal 1008.9 kg/m$^3$ in September), the sinking is 180-200 m.

In its following path, the flow have a different dynamic, thus another analytical model to describe the flow is presented (section 3.2).

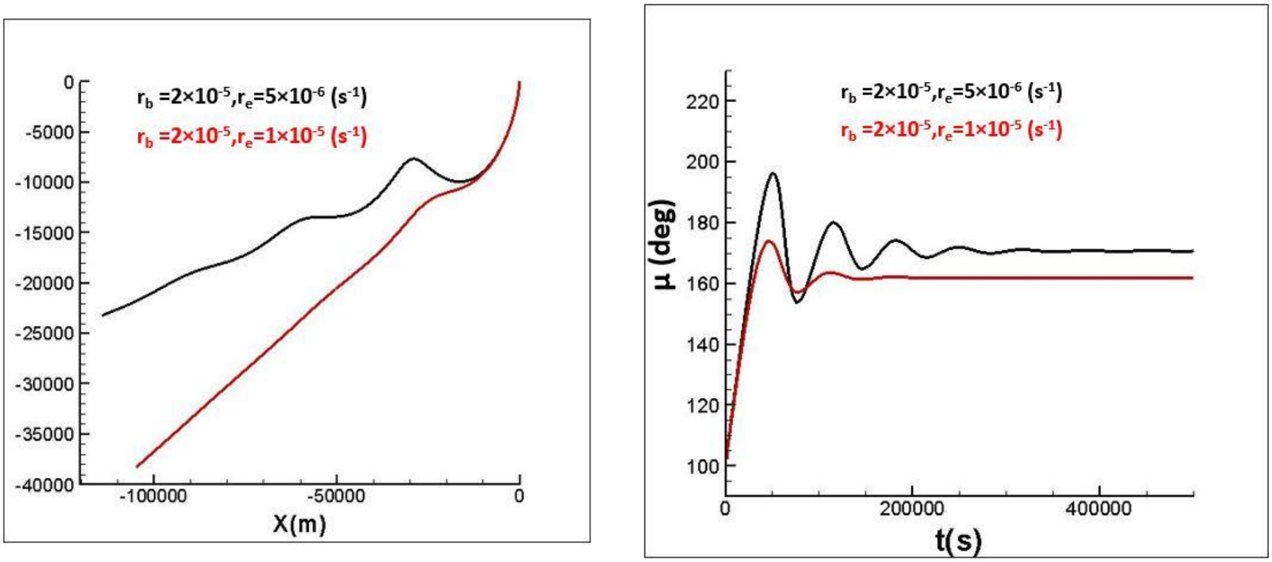


**Figure12:** The flow paths (southwards, based on local coordinates used, see model descriptions above, *t*~ 3 day) and its angle from eastward direction of the flow with different coefficients of entrainments. It should be noted that the scale of two axes is not the same.

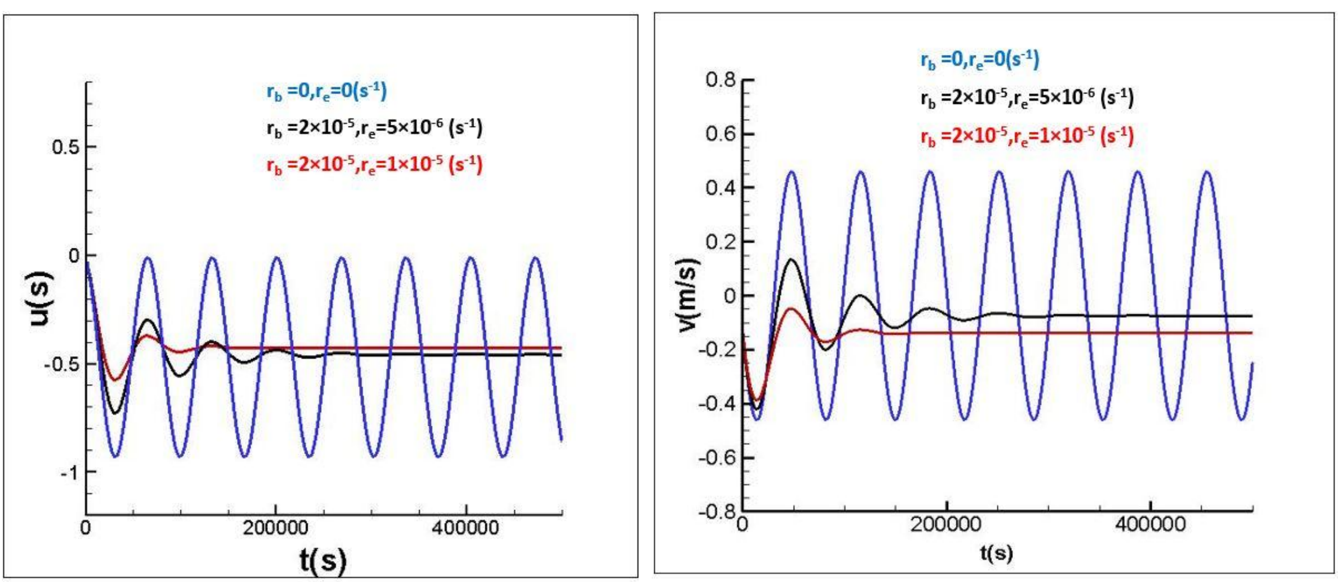


**Figure13:** Comparison of the velocity components with different coefficients of entrainments.

**Table 2:** Boundary current parameters and variables obtained from the numerical model (see text).

| | $g'$ (m/s$^2$) | $v_p$(m/s) | $u_p$(m/s) | $u_{t\to\infty}$ (m/s) | $v_{t\to\infty}$(m/s) | $\mu$(deg) | $\lambda$(deg) |
|---|---|---|---|---|---|---|---|
| **NOV** | 0.00222 | -0.12 | -0.044 | -0.12 | -0.119 | 160 | 107 |
| **JAN** | 0.00239 | -0.133 | -0.047 | -0.13 | -0.13 | 160 | 109.60 |
| **MAY** | 0.00251 | -0.147 | -0.031 | -0.135 | -0.135 | 160 | 101.91 |
| **SEP** | 0.00241 | -0.19 | -0.078 | -0.132 | -0.13 | 160 | 112.32 |

### 3. 2Vorticity and potential vorticity (PV) over the sill

Here we consider the structure of fluid flowing on the sill in terms of its vorticity and PV. Falcini and Salusti (2015) presented an analytic model for the Sicily channel: vorticity and PV equations based on the stream-tube model (Smith, 1975; Killworth, 1977). To deal with this, they used ($\xi$, $\psi$) coordinate system, a modified form of that used by Astraldi et al. (2001). In this frame, $\xi$ is the along-flow coordinate and $\psi$ is the cross-flow coordinate (see Figure 1 in Smith, 1975). In this method, friction and mixing effects are considered for estimation of potential vorticity whereas other models assume a zero-PV flow (Whitehead et al., 1974).They presented two formulas to calculate vorticity and potential vorticity (5and 6).Formulas are based on a homogeneous bottom water vein and using shallow water theory (over bars indicate cross sectional averages). To obtain the formula, the bottom water is assumed to be well mixed and the flow has a strong axial velocity nearly uniform over the cross section of the stream and also the cross-stream scale is assumed to be much smaller than the local radius of curvature of the streamline axis.

$$\frac{\bar{\zeta}}{f} = \frac{\bar{u}_0}{\bar{u}} e^{-\int_0^{\xi} \frac{r}{\bar{u}} dx} \left( \frac{\bar{\zeta}_0}{f} + \frac{1}{\bar{u}_0} \int_0^{\xi} e^{\int_0^{x} \frac{r}{\bar{u}} dx'} \left[ \frac{\bar{u}}{\bar{h}} \frac{\partial \bar{h}}{dx} - \frac{E}{\bar{h}} \right] dx \right. \qquad \textbf{(5)}$$

$$\Pi = e^{-\int_0^{\xi}\frac{\Gamma}{u}dx}\left[\Pi_0 - \int_0^{\xi} e^{\int_0^{x}\frac{\Gamma}{u}dx'}\frac{r\zeta}{hu}dx\right] \qquad \textbf{(6)}$$

Where $\Gamma=\frac{\boldsymbol{E}}{\boldsymbol{h}}$.

Here $\zeta$ and $\Pi$ are respectively the mean relative vorticity and potential vorticity, $h$ is the layer thickness and $\partial h/\partial x$ is slopes of the isopycnals, $\zeta_0$ and $\overline{u_0}$ are receptively the initial vorticity and velocity. To be applicable, some terms in Eq.5 are considered as cross sectional averages. Three terms are significant in vorticity: a stretching term, the entrainment effect, and friction. In 5 and 6, some symbols has been changed based on the present work. To estimate all parameters in these formulas, we use 5 transects from strait (I) to the southern area (V) (figure 16).Typically, for November in transect III $\Delta h$=180 m,$\Delta x$=38 km, $\bar{u}$=0.11 m/s, $\bar{h}$=180 m, are estimated. In the calculation of $r_b$, based on $Ri$ number similar to that in section 3.1, $r_b=2\times10^{-5}$ (1/s) and $r_e=4\times10^{-6}$(for transect II), $8\times10^{-7}$(for transect III) are calculated based on formulas in table 1(figure 14). In transect IV and V, $r_e$~0 because of large $Ri$~ 40 to 50. Using Eqs. 5 and 6, profiles of $\zeta$ and $\Pi$ are plotted in figures 15 as functions of $\xi$ along the steam tube.

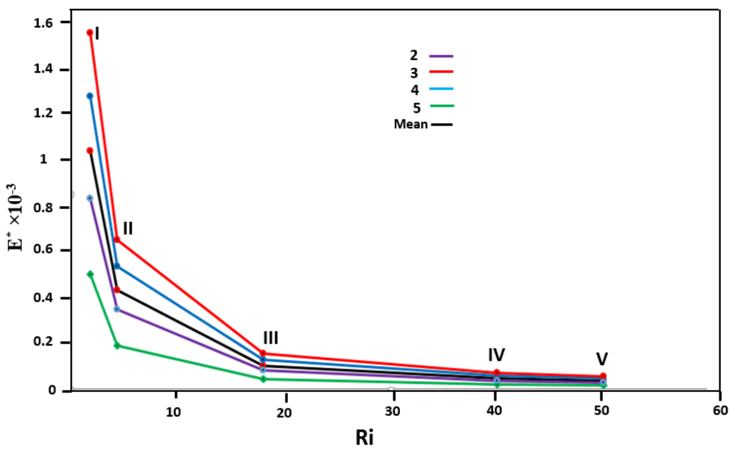


**Figure 14:** changes of entrainment coefficients based on different Richardson numbers for May in transects shown in figure 16. The formulas in table 1 are used to estimate $E^*$ (the numbers refer to the equation numbers in table 1). To use $E^*$ in Eq. 5and 6, mean values for $E^*$ is also estimated (black).

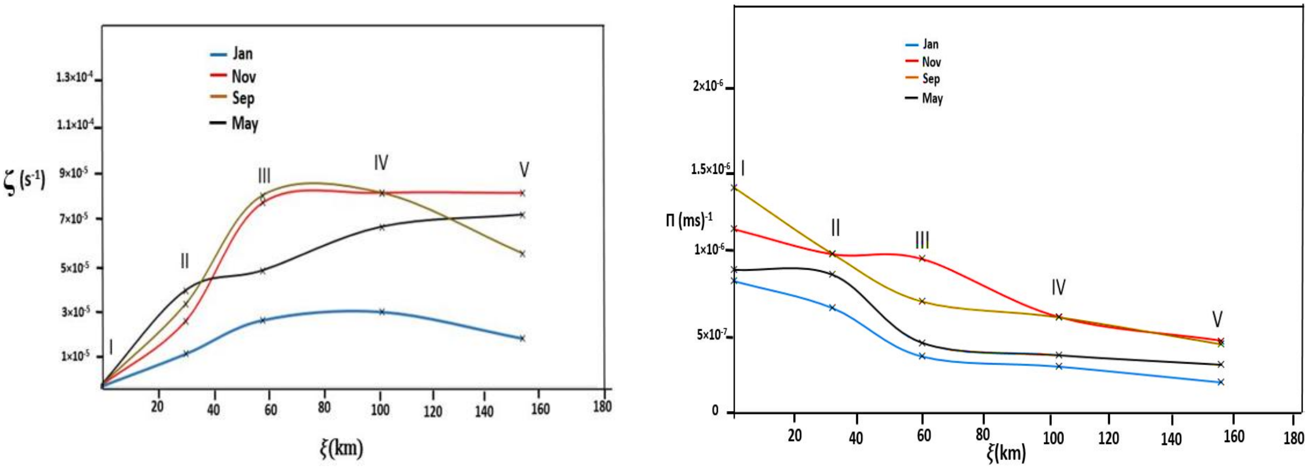


**Figure 15:** Changes in $\zeta (s^{-1})$ and $\Pi$ $(m^{-1}s^{-1})$ along the flow based on Eqs. 5 and 6.

Figure 15illustratesthat $\zeta$ values increase from I to V, because of stretching term in Eq. 5, although Sep and Jan values have different behaviour in transect IV to V. However after the transect III, the changes are not considerable, because the depth does not vary significantly (stretching term) and entrainment have been ignored as *Ri* is large after this transect. The month of November has the maximum value of vorticity of about $8.5\times10^{-5}$ (1/s) in transect V, although the Jan. value has minimum vorticity among other months and also the changes are very little after transect III. When it comes to $\Pi$, the graph shows decreases from I to IV, but after IV the $\Pi$ values are almost constant. For example, the changes of $\Pi$ over sill are about $7\times10^{-7}$ $(m^{-1}s^{-1})$ and $4\times10^{-7}(m^{-1}s^{-1})$ for Sep. and Jan. respectively, due to bottom friction and entrainment.

### 3.2.1 A model for the trapped flow

As the flow enters the southern Caspian Sea basin, it adjusts into an internal Quasi-geostrophic flow, because of topography in the southern Caspian basin (see Figure 16). When moving along the topography of the sloping sea bed, the governing equations of steady flow and similar assumptions as for the analytical model above, such as being homogeneous, and steady, with bottom friction (see section 3.1) are as follows:

$$\begin{aligned} fv &= g'\frac{\partial h}{\partial x} - r_b u \\ -fu &= g'\frac{\partial h}{\partial y} - r_b v \end{aligned} \qquad \textbf{(7)}$$

No mixing is an assumption due to flow entrainments near its boundaries due to $Ri$~50 ($E$=0, or $r_e=0$). Where now $u$ and $v$ are respectively the eastward and northward velocity components (see Figure16), $g´$ is the reduced gravity, $r_b$ is the friction coefficient (considered 0.00002 $s^{-1}$), and $\partial h/\partial x$, $\partial h/\partial y$ are slopes of the isopycnals of the overflow, related to the pressure gradient. From equation (7) it follows, assuming $\partial h/\partial y << \partial h/\partial x$:

$$\zeta = \frac{g'}{f + \frac{r_b^{\,2}}{f}} \frac{\partial^2 h}{\partial x^2} \qquad \textbf{(8)}$$

Potential vorticity is defined as:

$$\Pi = \frac{\zeta + f}{h} \qquad \textbf{(9)}$$

After substituting Eq. (8) in Eq. (9), an equation for $h$ is obtained.

$$\frac{\partial^2 h}{\partial x^2} = \beta^2 h - \gamma$$

Where:

$$\beta^2 = \left(\frac{f + \frac{r^2}{f}}{g'}\right)\Pi$$

$$\gamma = \left(\frac{f + \frac{r^2}{f}}{g'}\right) f$$

To estimate Π in transect D, we assume that $\Pi_V \sim \Pi_D$ because after the sill the flow depth is not changing and entrainment effect is almost zero. On the other hand, the bottom friction is important, however due to the short distance between D and V (figures 16 and 2), we use this assumption and overlook this effect. The solution of $h$ equation is as follows which is also shown in Figure 16:

$$h = c_1 e^{\beta x} + c_2 e^{-\beta x} + \frac{\gamma}{\beta^2} \qquad \textbf{(10)}$$

Where $c_1$and $c_2$are constants determined by the conditions that at the near-shore boundary($x=0$) the flow vanishes, therefore $x$ derivative of $h$ near the shore is negligible. (See Figure 16, and Figure 17which was used to derive values for these conditions); using these boundary conditions gives:

$c_1=c_2=c$

Hence, according to the equation, at $x$=0, $h_1$=2$c$+$\frac{\gamma}{\beta^2}$ and at $x$=$R$, $h_R$=c ($e^{\beta R}$ + $e^{-\beta R}$) +$\frac{\gamma}{\beta^2}$ then:

$$R = \frac{1}{\beta}\cosh^{-1}\left(\frac{h_R - \frac{\gamma}{\beta^2}}{h_1 - \frac{\gamma}{\beta^2}}\right) \qquad \textbf{(11)}$$

$\beta$ is is the scale of the flow. Using equation 11 and also the result of the graph (figure17), the Rossby deformation radius is then calculated (Table 3).

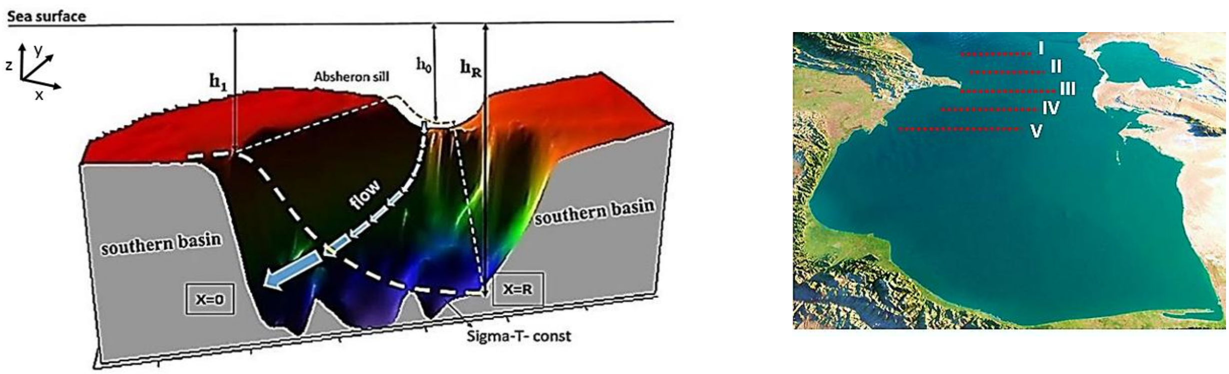


**Figure16**: The parameters of the outflow model, a typical isopycnal surface is shown after the sill with corresponding $h$ values found from the density fields such as shown in Figure17(left) (Axes are in right-hand coordinates) and the locations of transects to estimate the changes of vorticity and PV (right).

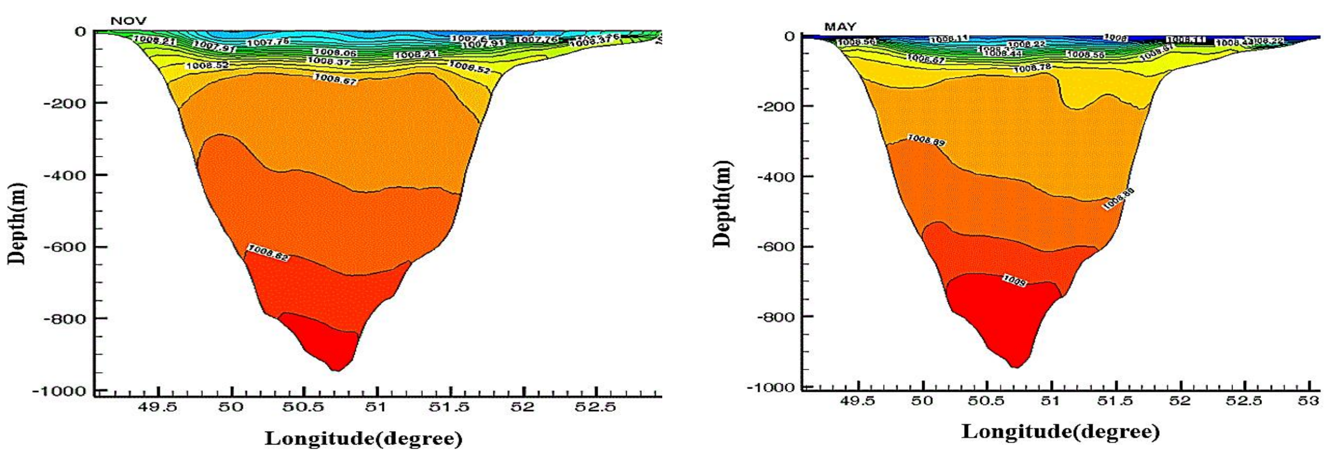


**Figure17**: Density fields along transect D in May (right) and Nov.(left).

**3.2. 1.1** ***Results of the analytical model for trapped current***

This model is presented for the trapped flow after Absheron sill due to Coriolis effect. In this present work, due to the fact that we consider the friction and entrainment, the potential vorticity is not conserved, in contrast with the analysis of Bidokhti and Ezam (2009) for the Persian Gulf outflow. To calculate the changes in potential vorticity, we use the method of Falcini and Salusti used in Sicily Channel. Results show that the Rossby deformation radius (length, $\sim\beta^{-1}$) or the effective width of the flow directly depends on the drag coefficients and reduced gravity which varies for different seasons (based on Eq.11). The smallest and largest widths (Rossby lengths) of the flow are for January and May respectively (table 3).According to the results, Rossby deformation radius varies from 17 to 30 km in different seasons. The results illustrate that the decrease in potential vorticity increases the flow Rossby deformation radius, which means that when we use initial vorticity on strait ($\Pi_I \sim \Pi_D$) the radius will decrease. For instance, in September we assume that the $\Pi_I \sim \Pi_D$ similar to previous work Bidokhti and Ezam(2009); the radius is calculated about 12 km. Due to the results, we can predict that Rossby deformation radius will increase in another location of the southern Caspian sea (near the Iranian coast), transect E in figure 2 because the bottom friction decrease $\Pi_E$ rather than $\Pi_D$. The numerical model (figure 9) confirms this prediction. As a result, Eq.7 and 8 can predict the changes of vorticity correctly over and after the Absheron sill. In order to evaluate the accuracy of the analytical model, the Rossby deformation radius is directly estimated from the numerical simulations. As shown in table 3, the analytical model also predicts this but with slightly smaller value. These results are based on certain assumptions used in these models, hence some errors are predictable. For example, due to what was mentioned ,we assume that $\Pi_V \sim \Pi_D$, however, in reality is $\Pi_D < \Pi_V$. As a result, the Rossby deformation radius is underestimated due to decreasing in potential vorticity that increases the flow Rossby deformation radius.

**Table 3:** Boundary trapped current model parameters (see Figure16 and transect D in figure 17) and values of *R*. The last column shows that direct calculation from the result of numerical model.

| | $h_0$(m) | $h_1$(m) | $h_R$ (m) | ***R*** **(km) Analytical** | ***R (km) Numerical*** |
|---|---|---|---|---|---|
| **NOV** | 120 | 270 | 400 | 17 | 18 |
| **JAN** | 150 | 440 | 485 | 15 | 16 |
| **MAY** | 110 | 300 | 400 | 30 | 34 |
| **SEP** | 140 | 430 | 570 | 25 | 35 |

### 3.3 Flushing times andthe volumes of dense water calculations

In this section, as we derive the parameters of the overflow, a relation is presented for the calculation of the abyssal volume flow rate between the two basins of the Caspian Sea via the Absheron Strait. This is given by (12) in which *v* is the mean magnitude of geostrophic velocity of the overflow and *ds* is an element of its cross section area.

$$Q_V = \int v ds \qquad \textbf{(12)}$$

Due to the parabolic form of the bottom topography of Absheron Strait, its geometry of the dense overflow in this valley like shape (Figure18) can be given by:

$$\begin{aligned} Z &= ax^2 + bx + c \\ h' &= Ae^{-\alpha x} \end{aligned} \qquad \textbf{(13)}$$

Where *a*, *b*, *c*, *A* and *α* are assumed to be constant. We consider the new definition for isopycnal in this part (*h´*) because Strait is narrow and the shape of its isopycnal lines is simpler than the current in the southern Caspian Sea. Apart from this, the isopicnal line slope is not zero to calculate the constant value (for estimation of h) similar to section 3.2.1.

Due to the fact that *Z* and *h´*(isopycnal line) in graph (Figure18) are from $L_1$to $L_2$we can calculate *h´* and *Z* values at ($x=L_1$) and ($x=L_2$), Substituting Eq. (13) in Eq. (12) and using these assumptions and that *v*, the geostrophic flow speed, is given by the slope of *h´* in x direction, we have:

$$Q_V = \frac{g'}{f}\frac{H_1 - H_2}{L_2 + L_1}\left[\left(-\frac{A}{\alpha}(e^{-\alpha L_2} - e^{\alpha L_1}\right) - \frac{a}{3}(L_2^3 + L_1^3) - \frac{b}{2}(L_2^2 - L_1^2)\right] \qquad \textbf{(14)}$$

Where:

$$a = \frac{H_2 L_1 + H_1 L_2}{L_1(L_2^2 + L_1 L_2)}$$

$$b = \frac{H_2 L_1 + H_1 L_2}{L_2^2 + L_1 L_2} - \frac{H_1}{L_1}$$

If we assume that $L = \frac{|L_1|+|L_2|}{2}$, we have

$$Q_V = \frac{g'}{f}\frac{H_1 - H_2}{L_2 - L_1}\left[\frac{2A}{\alpha}\sinh(\alpha L) - \frac{2}{3}aL^3\right] \qquad \textbf{(15)}$$

Where:

$$a=\frac{H_2+H_1}{2L^2}$$

$$b=\frac{H_2-H_1}{2L}$$

$$A=\frac{H_1}{e^{\alpha L}}$$

$$\alpha=-\frac{1}{2L}Ln\frac{H_2}{H_1}$$

To obtain the Eq. 15, we defined $L$ based on $L_1$ and $L_2$ because $L_2 \neq L_1$. Although the minimum of $Z$ is not exactly at $x$=0, as it does not create large error. To show this reality, the $Q_V$ is calculated separately with Eq. 14 and 15.The results show that the error is about 2-5 percent rather than using any assumptions (Eq.14).

To calculate the mean monthly volume flow rate of the deep current that enters the southern basin of the Caspian Sea, we assume that its density is greater than 1008.78kg/m$^3$, the average density (for different seasons) of the flow upper boundary (e.g. Figure19)and use equation (17) and figure19for this purpose.

For the times that the middle and southern basins are filled, first the volumes of middle ($V_M$), and southern ($V_S$) basins (see Figure 18) are calculated below three levels ($z$=0,$z$=-100, and $z$=-150 m, the approximate depth of the Absheron sill that is more appropriate only for southern basin), then if we assume the same annual mean value $Q_V$ for both basins, these filling times are estimated. The results of these calculations and comparisons between them in different seasons are given in Tables 4and 5.The results show that the maximum and minimum flow rates of abyssal water that enter the Southern Caspian Sea are in May and November respectively. In order to check the accuracy of Eq. 15, the $Q_V$ is directly calculated from the numerical simulations without any assumptions. As shown in table 4, the model predicts this value which is less than the analytical value. This underestimation can be due to the fact that we use some assumptions to obtain Eq. 15. The velocity used is the geostrophic velocity and the isopycnal line is simplified. Apart from this, some errors comes from the choice of 1008.78 kg/m$^3$ contour as its position changes for different months. If we consider the contour 1008.9 kg/m$^3$, it is appropriate for some months like January, but it is not useful for November because the maximum contour is 1008.8 kg/m$^3$ for this month. This method can create some error in some month, for example for January; the contour does not exactly reach the bottom. To solve this problem we can use special contour for each month, however we ignore this method because it is not useful to calculate $Q_V$ under the same conditions for all month. The flushing time is estimated based on the direct calculation from the numerical simulations. The results show that the flushing time is about 6-7(middle basin) and 13-14 (southern basin) years for the numerical simulations based on $z$=0. As a result, the Eq. 15 can be useful to estimate the volume flux of water in the strait, particularly in this oceanic environment without ADCP data. For example in Persian Gulf, there are many CTD data on the Hormuz strait based on Bidokhti and Ezam(2009) but there is not any ADCP data, so the result of this paper can be used to estimate the volume of deep water in their work.

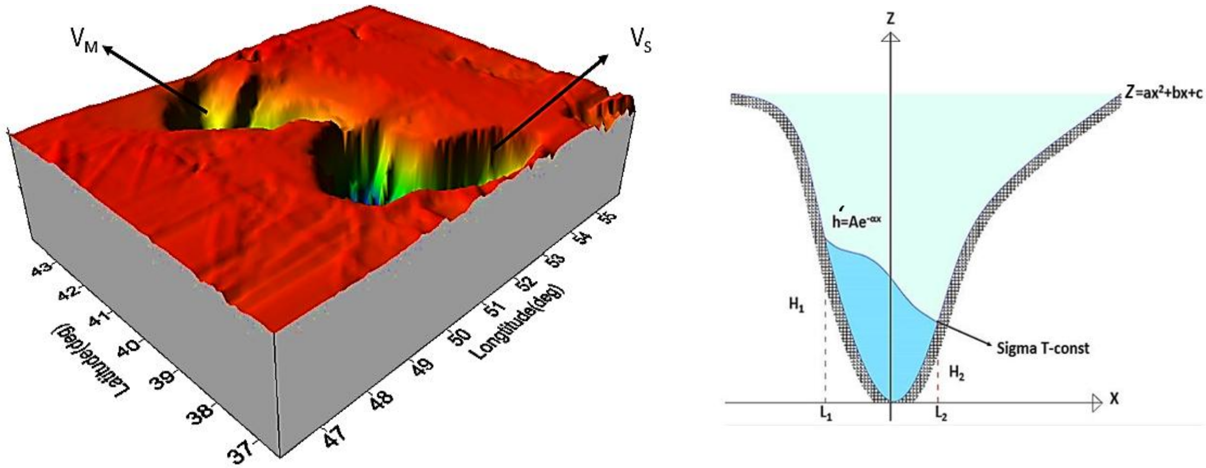


**Figure18:** The modelling bathymetry used and the scheme of the topography with a typical isopycnal and model parameters.

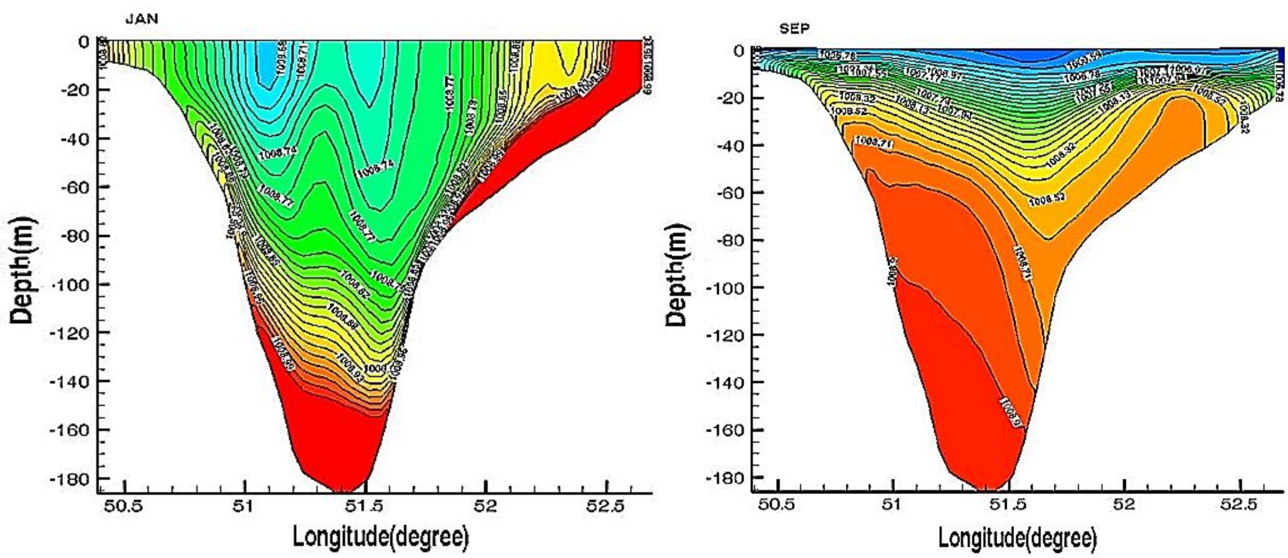


**Figure19**: Typical density fields along transect A for Jan. (left) and Sept. (right) from which we calculate the flow rates.

**Table4:** The model boundary current parameters (1 *Sv*=$10^6$ $m^3$/s) for different months. The last column (red symbol) show direct calculation from the numerical model

| | $H_1$ (m) | $H_2$(m) | *2L* (m) | $Q_V$(Sv) Analytical | $Q_V$(Sv) Numerical |
|---|---|---|---|---|---|
| **NOV** | 55 | 10 | 19000 | 0.016 | 0.034 |
| **JAN** | 145 | 85 | 32000 | 0.115 | 0.15 |
| **MAY** | 145 | 55 | 34000 | 0.146 | 0.17 |
| **SEP** | 135 | 45 | 27500 | 0.116 | 0.16 |

**Table 5**: Flushing times of the middle($T_M$) and the southern ($T_S$) basins (using an annual average volume flow rate (,$Q_V$) below three levels.

| Level | $V_M$(m$^3$×10$^{13}$) | $V_S$(m$^3$×10$^{13}$) | $T_M$(year) | $T_S$(year) |
|---|---|---|---|---|
| ***z*=0 (sea surface)** | 2.55 | 5.12 | 8.35 | 16.77 |
| ***z*=-100** | 1.09 | 4.13 | 3.57 | 13.5 |
| ***z*=-150** | 0.36 | 3.62 | 1.17 | 11.85 |

## 4. Conclusions

The results of observations and numerical simulations showed that there is an abyssal flow from the middle to the southern basins of the Caspian Sea. The density difference between the deeper water of the middle basin and that of southern basin leads to an overflow gravity current over the Absheron sill. This difference is mainly due to the temperature difference between deeper parts of these two basins, as a result of cold water initially sinking in the northern part of this Sea, at about 48 degrees latitude, that fills first the middle basin and then overflows towards the southern basin. In the autumn and winter, surface water cools and its density is increased and then sinks to the deep part of the middle basin, as the deep convection process in high latitude oceans. Winter storms and cold wind provide the cooling of this rather high-latitude shallow water in the northern basin.

Analytical models for the gravity driven flow over the sloped bed of the Absheron sill and that of subsequent trapped flow, were used to estimate typical mass transport and flushing times of the deep water basins of this Sea. The model for the gravity driven flow over a sloped bed has inertial, Coriolis and frictional forces included. In its initial stage the flow has some oscillations of inertial type with typical local inertial period at this latitude. After this varying behaviour, the flow adjusts itself moving south as a gravity driven topographically trapped current, spiralling into deeper parts due to bottom friction and entrainment. It always tends to move toward the western shores of this Sea, mainly due to the Coriolis force that shifts it to the right. Such flow is important in the abyssal circulation and ventilation of the deep southern basin of the Caspian Sea. The model for the determining Rossby length of the flow showed that it varies for different seasons. For vorticity and potential vorticity of the flow, the formulas which are presented by Falcini and Salusti(2015) are used to estimate the changes of relative vorticity and potential vorticity over Absheron sill, that are used in the analytical trapped current.

Results also showed that nearly $3.05\times10^{12}$ m$^3$of water per year by this abyssal flow can enter the Southern basin giving a typical flushing time of about 15 to 20 years which are of the same order as those estimated by Peeters et al. (2000), as the southern Caspian basin ecosystem is strongly dependent on this flow.

The northern and middle Caspian Sea basins have become important areas for oil and gas explorations (especially the Absheron shallow Strait area) and marine transport nowadays. Since the Caspian Sea is an enclosed sea, the adverse effects of such activities may particularly affect the deep part of these Caspian Sea basins. For this reason, it is recommended that more detailed observational data are collected in the deep parts of the southern and middle basins of the Caspian Sea, by joint projects with neighbouring countries. More extensive and high resolution observational data and numerical simulations are required to find more details of the outflow structure over and around the Absheron sill (Strait) and the deeper parts of this Sea basins.

**Acknowledgment**

The financial support of University of Tehran, while doing this work is greatly acknowledged.

**References**

Arakawa, A.& Suarez, M. J. (1983). Vertical differencing of the primitive equations in sigma coordinates. *Monthly Weather Review*, *111*(1), 34-45.

Astraldi, M., Gasparini, G. P., Gervasio, L.& Salusti, E. (2001). Dense water dynamics along the Strait of Sicily (Mediterranean Sea). Journal of Physical Oceanography, 31(12), 3457-3475.

Ashida, K.& Egashira, S. (1975, May). Basic study on turbidity currents. In Proceedings of the Japan Society of Civil Engineers (Vol. 1975, No. 237, pp. 37-50). Japan Society of Civil Engineers.

Aubrey, D.G., Glushko, T.A. & Ivanov, V.A.(1994). North Caspian Basin: Environmental status and oil and gas operational issues, *Report for Mobil-oil, 650 pages.*

Aubrey, D.G.(1994). Conservation of biological diversity of the Caspian Sea and its coastal zone. A proposal the Global Environment Facility, *Report to GEF, 250 pages.*

Baringer, M. O. N.& Price, J. F. (1997). Mixing and spreading of the Mediterranean outflow. *Journal of Physical Oceanography*, *27*(8), 1654-1677.

Bidokhti, A. A.& Ezam, M. (2009). The structure of the Persian Gulf outflow subjected to density variations. *Ocean Science*, *5*(1), 1-12.

Bondarenko, A. L.(1993). Currents of the Caspian Sea and Formation of Salinity of the Waters of the North Part of the Caspian Sea [in Russian],*122 pp., Nauka, Moscow, Russia.*

Britter, R. E.& Linden, P. F. (1980). The motion of the front of a gravity current travelling down an incline. *Journal of Fluid Mechanics*, *99*(3), 531-543.

Cheng, R. T., Ling, C. H., Gartner, J. W.& Wang, P. F. (1999). Estimates of bottom roughness length and bottom shear stress in South San Francisco Bay, California. *Journal of Geophysical Research: Oceans*, *104*(C4), 7715-7728.

Dickson, R. R., Gmitrowicz, E. M.& Watson, A. J. (1990). Deep-water renewal in the northern North Atlantic. *Nature*, *344*(6269), 848-850.

Ellison, T. H.& Turner, J. S. (1959). Turbulent entrainment in stratified flows. *Journal of Fluid Mechanics*, *6*(3), 423-448.

Falcini, F.& Salusti, E. (2015). Friction and mixing effects on potential vorticity for bottom current crossing a marine strait: an application to the Sicily Channel (central Mediterranean Sea). Ocean Science, 11(3), 391-403.

Fogelqvist, E., Blindheim, J., Tanhua, T., Østerhus, S., Buch, E.& Rey, F. (2003). Greenland–Scotland overflow studied by hydro-chemical multivariate analysis. *Deep Sea Research Part I: Oceanographic Research Papers*, *50*(1), 73-102.

García, M. H. (1993). Hydraulic jumps in sediment-driven bottom currents. Journal of Hydraulic Engineering, 119(10), 1094-1117.

Ghaffari, P.& Chegini, V. (2010). Acoustic Doppler Current Profiler observations in the southern Caspian Sea: shelf currents and flow field off Feridoonkenar Bay, Iran. *Ocean Science*, *6*(3), 737.

Ghaffari, P., Isachsen, P. E.& LaCasce, J. H. (2013). Topographic effects on current variability in the Caspian Sea. *Journal of Geophysical Research: Oceans*, *118*(12), 7107-7116.

Girton, J. B.& Sanford, T. B. (2003). Descent and modification of the overflow plume in the Denmark Strait. *Journal of Physical Oceanography*, *33*(7), 1351-1364.

Griffiths, R. W. (1986). Gravity currents in rotating systems. *Annual Review of Fluid Mechanics*, *18*(1), 59-89.

Gunduz, M.& Özsoy, E. (2014). Modeling seasonal circulation and thermohaline structure of the Caspian Sea. *Ocean Science*, *10*(3), 459-471.

Ibrayev, R. A., Özsoy, E., Schrum, C.& Sur, H. I. (2010). Seasonal variability of the Caspian Sea three-dimensional circulation, sea level and air-sea interaction. *Ocean Science*, *6*(1).

Ismailova, B. B. (2004). Geoinformation modeling of wind-induced surges on the northern–eastern Caspian Sea. *Mathematics and Computers in Simulation*, *67*(4), 371-377.

Johnson, G.C. and Sanford, T.B. (1992). Bottom and interfaeial stresses on the Mediterranean outflow. Tenth Symposium on Turbulence and Diffusion. Portland, Oregon. *American MeteorologicalSociety, 105-106.*

Kara, A. B., Wallcraft, A. J., Metzger, E. J.& Gunduz, M. (2010). Impacts of freshwater on the seasonal variations of surface salinity and circulation in the Caspian Sea. *Continental Shelf Research*, *30*(10), 1211-1225.

Karamzadeh, N. (2004). Experimental investigation of water entrainment into density current.M. Sc. Thesis, Shahid Chamran University, Ahvaz, Iran.

Kashefipour, S., Kooti, F.& Ghomeshi, M. (2010, June). Effect of reservoir bed slope and density current discharge on water entrainment. In Environmental Hydraulics, Two Volume Set: Proceedings of the 6th International Symposium on Enviornmental Hydraulics, Athens, Greece, 23-25 June 2010 (p. 195). CRC Press.

Kessel, T. V.& Kranenburg, C. (1996). Gravity current of fluid mud on sloping bed. Journal of Hydraulic Engineering, 122(12), 710-717.

Killworth, P. D. (1977). Mixing of the Weddell Sea continental slope. Deep Sea Research, 24(5), 427-448.

Luyten, P.J., Jones, J.E., Proctor, R., Tabor, A., Tett, P.&Wild-Allen, K. (1999). COHERENS- A coupled hydrodynamical-ecological model for regional and shelf seas: user documentation, MUMM Rep., *Management Unit of the Mathematical Models of the North Sea.*

Mazaheri, S., Kamranzad, B.& Hajivalie, F. (2013). Modification of 32 years ECMWF wind field using QuikSCAT data for wave hindcasting in Iranian Seas. *Journal of Coastal Research*, *65*(sp1), 344-349.

Peeters, F., Kipfer, R., Achermann, D., Hofer, M., Aeschbach-Hertig, W., Beyerle, U.& Fröhlich, K. (2000). Analysis of deep-water exchange in the Caspian Sea based on environmental tracers. *Deep Sea Research Part I: Oceanographic Research Papers*, *47*(4), 621-654.

Price, J. F. & Baringer, M. O. N. (1994). Outflows and deep water production by marginal seas. *Progress in Oceanography*, *33*(3), 161-200.

Shiea, M., Chegini, V.& Bidokhti, A. A. (2016). Impact of wind and thermal forcing on the seasonal variation of three-dimensional circulation in the Caspian Sea,IJMS, Vol. 45 (05),671-686.

Smith, P. C. (1975, December). A streamtube model for bottom boundary currents in the ocean. In *Deep Sea Research and Oceanographic Abstracts*(Vol. 22, No. 12, pp. 853-873), Elsevier.

Terziev, F. S., Kosarev, A.& Kerimov, A.A.(1992). The Seas ofthe USSR. Hydrometeorology and Hydrochemistry of the Seas, vol. VI,the Caspian Sea, Issue 1: Hydro meteorological Conditions, Gidrometeoizdat, St. Petersburg, Russia.

Whitehead, J. A., Leetmaa, A.& Knox, R. A. (1974). Rotating hydraulics of strait and sill flows. *Geophysical and Astrophysical Fluid Dynamics*, *6*(2), 101-125.